

Validation of the plasma-wall self-organization model for density limit in ECRH-assisted start-up of Ohmic discharges on J-TEXT

Jiaxing Liu¹, Ping Zhu^{1,2*}, Dominique Franck Escande³, Junli Zhang¹, Donghui Xia^{1*}, Yuhan Wang¹, Jiaming Wang¹, Qinghu Yang¹, Jiangang Fang¹, Li Gao¹, Zhifeng Cheng¹, Zhipeng Chen¹, Zhoujun Yang¹, Zhongyong Chen¹, Yonghua Ding¹, Yuan Pan¹ and the J-TEXT team[‡]

¹International Joint Research Laboratory of Magnetic Confinement Fusion and Plasma Physics, State Key Laboratory of Advanced Electromagnetic Engineering and Technology, School of Electrical and Electronic Engineering, Huazhong University of Science and Technology, Wuhan, 430074, China.

²Department of Engineering Physics, University of Wisconsin-Madison, Madison, Wisconsin, 53706, United States of America.

³Aix-Marseille Université, CNRS, PIIM, UMR 7345, Marseille, France.

E-mails: zhup@hust.edu.cn, xiadh@hust.edu.cn

18 April 2023

Abstract. A recently developed plasma-wall self-organization (PWSO) model predicts a significantly enhanced density limit, which may be attainable in tokamaks with ECRH-assisted ohmic startup and sufficiently high initial neutral density. Experiments have been conducted on J-TEXT to validate such a density limit scenario based on this model. Experimental results demonstrate that increasing the pre-filled gas pressure or ECRH power during the startup phase can effectively enhance plasma purity and raise the density limit at the flat-top. Despite the dominant carbon fraction in the wall material, some discharges approach the edge of the density-free regime of the 1D model of PWSO.

Keywords: Density limit, radiation, plasma wall interaction, ECRH, J-TEXT

1. Introduction

A high plasma density in a fusion device is crucial for fulfilling the Lawson criterion for ignition. However, there exists an upper limit to this density, above which a disruption may occur, leading to the termination of the discharge. Since this density limit sets a stringent bound on the stable performance and ignition regimes of a tokamak, its scaling and the associated physics has been a subject of primary interests.

[‡] See the author list of "N. Wang et al 2022 Advances in physics and applications of 3D magnetic perturbations on the J-TEXT tokamak, Nucl. Fusion 62 042016"

For decades, people used the empirical scaling law for the tokamak density limit $n_{\text{GW}} (\text{m}^{-3}) = \frac{I_p (\text{MA})}{\pi a (\text{m})^2} \times 10^{20}$, where I_p is the plasma current and a is the minor radius [1, 2]. Recently, a power balance model considering radiation introduced a modified scaling for the density limit, $(I_p P / a^4)^{(4/9)}$, where P is the heating power [3, 4, 5]. This radiative scaling is in better agreement with the tokamak and reversed field pinch (RFP) experimental databases. The same model yields a good scaling for the stellarator too [3, 5, 6]. The primary factors influencing these power balance limits stem from impurity radiation, which is largely controlled by plasma-wall interactions [3, 4, 5]. This radiation affects the amount of heat reaching the limiter/divertor targets, subsequently determining the temperature in the target region. Additionally, the target region temperature significantly impacts impurity production, which in turn influences impurity radiation. This feedback mechanism forms the foundation of the recently proposed plasma-wall self-organization theory [7]. This self-organization mechanism yields a steady level of impurity radiation only when the plasma density is below a certain radiative limit [7]. A higher density limit is reached in stellarator when the start-up is performed by using higher ECRH power [8, 9]. This higher density limit might be due to their mode of breakdown at start-up phase: the massive use of ECRH power with high neutral density producing less impurities [3, 7]. Furthermore, in W7-X the effective plasma charge Z_{eff} decreases with ECRH power [10]. This suggests that increasing progressively and simultaneously the ECRH power and the initial neutral density could also decrease the initial production of impurities in tokamaks [7]. And this may increase the above radiative density limit.

In order to investigate the impact of start-up conditions, including pre-filled neutral gas pressure and ECRH power, on the flat-top density limit in ECRH assisted ohmic discharges, a series of experiments are conducted on the J-TEXT tokamak. The experimental results indicate that increasing either the pre-filled gas pressure or the ECRH power in the start-up phase leads to a reduction in impurity radiation, an increase in the boundary electron temperature during the flat-top phase, and an enhancement of the density limit in most of the shots. Besides, the density limit is calculated using PWSO 0D and 1D model with parameters of J-TEXT. The results demonstrated a general agreement with the experimental data under certain parameter assumptions.

The remainder of this paper is organized as follows: Section 2 introduces the experimental set-up. Section 3 details the experimental methods and presents the measurement results. Section 4 offers a comparison and analysis of the experimental and calculated results. Lastly, Section 5 concludes with a summary and discussion.

2. Experimental set-up

The J-TEXT tokamak is a medium sized iron-core tokamak with a major radius $R_0 = 1.05 \text{ m}$, minor radius $a = 25 - 29 \text{ cm}$, and a silicon-carbide-coated graphite limiter [11]. The typical J-TEXT discharge in the limiter configuration is performed with a toroidal magnetic field B_t of $\sim 2.0 \text{ T}$, a plasma current I_p of $\sim 200 \text{ kA}$, plasma density n_e of $1 - 7 \times 10^{19} \text{ m}^{-3}$, and an

electron temperature T_e of ~ 1 keV [11]. The Ohmic discharges begin with a reversed current closed at $t = 0.0$ ms to increase the rate of magnetic flux change. Then the capacitors bank, including the ionization capacitors, discharges to the ohmic coils to induce a toroidal electric field, ionizing the gas within the vacuum chamber. Following this, the capacitors for rapid build up of plasma current are turned on.

The material of limiter targets in J-TEXT is carbon whose chemical sputtering by hydrogen is not negligible in comparison to the physical sputtering [12]. The role of silicon carbide coating is to reduce the sputtering of carbon. In the following calculation concerning the sputtering function, its effects are neglected since the impurity radiation on J-TEXT primarily originates from carbon. The limiter target can absorb a large amount of gas in high electron density discharges, thus cleaning discharges have to be carried out during the experiments. Since non-standard start-up settings are used for this study, a noticeable amount of discharges fail or disrupt. Gas puffing can be applied to inject hydrogen with various pre-filled gas pressure and gas puffing rate. The ECRH system on J-TEXT was installed in 2019 [13]. Generated by a gyrotron, the maximum output power is 500 kW and the frequency is 105 GHz. The toroidal magnetic field range of the ECRH system operation is $1.7 \text{ T} \leq B_t \leq 2 \text{ T}$. The ECRH auxiliary heating system operates at the second harmonic frequency with X mode [14, 15].

The primary diagnostics for this experiment include the photo-diode array (PDA), Langmuir probe, polarimeter-interferometer (Polaris) system, and vacuum gauge. The arrangement of these diagnostic systems, as viewed from the top, is depicted in Fig. 1. The PDA array, responsible for measuring C_{III} and hydrogen-alpha radiations on the high field side, comprises 18 channels installed at the top of port 10. A Langmuir probe array at port 13 measures the electron temperature around the top limiter. The Polaris system is capable of measuring 17-channel line-averaged plasma electron density at different major radii [16]. The vacuum gauge quantifies the pre-filled gas pressure within the vacuum vessel.

3. Experimental results

3.1. Baseline discharge

A pure Ohmic start-up baseline discharge (#1082483) is shown in Fig. 2. The discharge starts at 0.0 s, with a toroidal magnetic field of 1.875 T and a plasma current of 120 kA. Hydrogen gas is injected after an electric pulse is sent to the gas puffing system, resulting in a neutral gas pressure of approximately 3 mPa at $t = 0$ s. During the current plateau period, gas injection continues until the plasma density limit of $0.7n_G$ is reached. At this point, the plasma density starts to decrease and then rapidly drops to zero, without any prior manifestation of MHD activities. More experimental details can be found in recent reports [14, 15].

3.2. Density limit parameter dependence

Many discharges are performed with varying pre-filled gas pressure and start-up ECRH power as shown in Fig. 3. These discharges are analyzed to obtain the dependence of density limit

n_{limit} on key parameters including the target region temperature T_t and the C_{III} radiation power. These experiments were completed on two experimental days, and the final density limit values achieved under identical input conditions may differ due to varying device setup states, such as the wall state, on different experimental days. However, this does not affect the overall law of the experimental results. The discharges shown in Fig. 4 and Fig. 5 have identical plasma current, toroidal magnetic field but differ in start-up conditions, either in terms of pre-filled gas pressure or ECRH power. The plasma temperature T_t values around the limiter target and impurity radiation power $R_{C_{\text{III}}}$ in Fig. 4 and Fig. 5 represent their average values over the time interval [200 ms, 250 ms], during which they are relatively stable. The C_{III} radiation and target region temperature at the current plateau phase can be adjusted by changing the start-up condition. The experimental data indicates that lower C_{III} radiation and higher target region temperature generally lead to a higher density limit, as shown in Fig. 4 and Fig. 5. Subsequently, two typical examples of varying gas pressure and ECRH power will be discussed in detail.

3.3. Typical discharge for changing gas pressure

Discharge #1083014 is performed with a higher pre-filled gas pressure than the baseline discharge. The neutral gas pressure P_{neu} at $t = 0$ s is approximately three times higher as shown in Fig. 2. The gas pressure of shot #1083014 remains higher than that of shot #1082483 during current ramping phase (Fig. 2). The C_{III} radiation power initially oscillates and eventually approaches a steady level over time in both discharges. The plasma target region temperature is higher in the discharge with higher gas pressure after the radiation power stabilizes. During the current plateau phase, hydrogen gas is injected at the same rate until the density limit disruption is triggered. A higher density limit of $0.745n_G$ is achieved in the discharge with higher pre-filled gas pressure.

3.4. Typical discharge for changing ECRH power

Another discharge, #1082481, is performed with the application of ECRH over the time interval $[-25 \text{ ms}, 20 \text{ ms}]$. The injected ECRH power is approximately 230 kW. Concurrently, the hydrogen gas is injected at the same rate with the baseline discharge until the density limit is reached. The injected ECRH power before $t = 0$ s ionizes the pre-filled gas and forms the so-called pre-plasma. The C_{III} radiation power oscillates and reaches a lower steady state than that of the baseline discharge. During the start-up phase, the temperature oscillation amplitude is slightly larger than that of the baseline discharge. And the steady target region temperature remains consistently higher. During the current plateau phase, the plasma density in this discharge increases at nearly the same rate as that of the baseline discharge but for an extended duration, ultimately reaching a higher density limit of $0.756n_G$.

4. Theory and experiment comparison

We further compare the predictions from the PWSO 0D and 1D models with the J-TEXT experimental results presented in the previous section.

4.1. PWSO 0D model and comparison

The basic idea of the PWSO theory (section 4.1 of [7]) is that the existence of a time delay in the feedback loop relating impurity radiation and impurity production on divertor/limiter plates yields a delay equation in the 0D model

$$R_+ = \alpha(P - R) \quad (1)$$

where P is the total input power to plasma, R the total radiated power, and R_+ the delayed radiation power during the next cycle of the feedback loop.

The coefficient α quantifies the radiation power R_+ generated by the impurity produced from the plasma-wall interaction that is proportional to the deposition of the outflow power $(P - R)$ onto the wall targets, which is modeled as [7]

$$\alpha = \frac{f\lambda}{aD_{\perp}T_t} I(T_t) \int_0^a rn(r) \text{Rad}[T(r)] dr \quad (2)$$

where a is the plasma radius, D_{\perp} is the perpendicular diffusion coefficient, T_t is the plasma temperature at the target plate location, f is the fraction of the sputtered atoms that reach the main plasma and become ionized at a distance λ inwards from the plasma target location, $\text{Rad}[T(r)]$ is the impurity radiation rate coefficient, and $I(T_t)$ is an average of the yield function of carbon $Y(E)$ over the energies of the impinging particles

$$I(T_t) = \sqrt{\frac{m}{2\pi T_t}} \int_0^{\infty} Y\left(\frac{mv^2}{2} + \gamma T_t\right) \exp\left(-\frac{mv^2}{2T_t}\right) dv \quad (3)$$

where γ is the total energy transmission coefficient [12], γT_t is a measure of the Debye shield length, and m is the ion mass. The fixed point of Eq.(1) $R = R_+$ corresponds to the plasma-wall self-organization equilibrium. The plasma-wall system is unstable for $\alpha > 1$ as predicted from Eq. (1). So the condition that the threshold $\alpha = 1$ establishes a radiation density limit

$$n_c = \frac{2D_{\perp}}{f\lambda \text{Rad}[T(r)]} \frac{T_t}{I(T_t)a} \quad (4)$$

which can be reached for a ratio of total radiated power to total input power as low as 1/2 [7]. If there is a detachment, the plasma temperature at the plates decreases as shown in Fig. 6, which makes α to vanish, since sputtering does too. This pushes the radiative density limit to very high values, especially when physical sputtering dominates the contribution to radiation. There are two basins of PWSO at the flat top of plasma current. The usual one is the regime of density limit corresponding to the higher temperatures of targets, whereas the other is the regime of density freedom corresponding to the lower temperatures of targets, in particular in machines where the target plates are made of high-Z materials.

The projectile particles in our experiments are deuterons and the target material is carbon. The yield function consists of two parts for the physical and chemical sputtering contributions. The interpolating functions for $Y_{\text{phy}}(E)$ at normal incidence are provided in the Eq. (15) of [17] for physical sputtering

$$Y_{\text{phy}}(E) = 0.042 \frac{Q(Z_2) \alpha^*(M_2/M_1)}{U_s} \frac{S_n(E)}{1 + \Gamma k_e \varepsilon^{0.3}} \times \left[1 - \sqrt{\frac{E_{\text{th}}}{E}} \right]^s \quad (5)$$

where the parameters on the right hand of Eq. (5) can also be found. Here the numerical coefficient 0.042 is in unit of \AA^{-2} , Z_1 and Z_2 are the atomic numbers, M_1 and M_2 are the masses of the projectile and the target atoms, respectively, S_n is the reduced nuclear stopping cross section, U_s is the surface binding energy of the target solid, k_e is the Lindhard electronic stopping coefficient, E is the projectile energy, E_{th} is the threshold energy for sputtering, ε is the reduced energy $E \frac{M_2}{M_1 + M_2} \frac{a_L}{Z_1 Z_2 e^2}$, the Γ factor has the form $W(Z_2) / \left(1 + (M_1/7)^3 \right)$, and W and Q are dimensionless fitting coefficients. The yield function $Y_{\text{che}}(E)$ for chemical sputtering is obtained from fitting the available experimental data in Fig. 3.8 of [12] and Fig. 6 of [18] using the least squares method

$$Y_{1,\text{che}}(E) = \begin{cases} a_1 E_1^2 + b_1 E_1 + c_1 & E_1 < E_{1,\text{inter}} \\ a_2 E_1 + b_2 & E_1 \geq E_{1,\text{inter}} \end{cases} \quad (6)$$

where $E_1 = \log_{10}(E)$, $Y_{1,\text{che}} = \log_{10} Y_{\text{che}}$, Y_{che} represents the chemical sputtering yield function. a_1, b_1, c_1, a_2, b_2 , and $E_{1,\text{inter}}$ are the fitting coefficients. The values of these coefficients can be found in Appendix A, along with a plot illustrating the fitted chemical sputtering yield function and the original data points. For our experiments on J-TEXT, the minor radius $a = 0.265$ m, and the impurity radiation rate $\text{Rad}[T(r)]$ is assumed to be a constant value 10^{-32}Wm^{-3} [4, 12]. We further assume that the perpendicular diffusion coefficient D_{\perp} of target impurities is $0.01 \text{m}^2 \text{s}^{-1}$, and one percent of the sputtered atoms penetrate the main plasma, undergoing ionization at a distance $\lambda = 0.01$ m away from the target. The maximum energy carried by the projectile particle is assumed to be 5000 eV, which is needed in the integral operation of Eq. (3). The relation between the density limit and the temperature of target for our experiments as predicted by the PWSO 0D model is thus calculated and shown in Fig. 7.

The PWSO 0D model predicts a density-free regime ($T_t \lesssim 2$ eV) and a density-limit regime ($T_t \gtrsim 2$ eV). In the density-free (density-limit) regime, the density limit increases with the decrease (increase) of the target region plasma temperature. J-TEXT experimental results are located in the density-limit regime, which qualitatively agree with the PWSO 0D model predictions.

4.2. PWSO 1D model and comparison

A more detailed evolution of the radiation power and the temperature towards the PWSO equilibrium profiles can be obtained from the PWSO 1D model (see appendix C of [7]).

The impurity density and the plasma temperature evolution can be determined from the following 1D transport equations

$$\partial_t n_i - D \partial_x^2 n_i = C_i [\partial_x T (r_{\text{LCFS}}, t - \tau_{\text{delay}}) + T'_{\text{loss}}] \delta(x - a + \lambda), \quad (7)$$

$$n \partial_t T - K \partial_x^2 T = C_T T^{3/2} + P_{\text{add}} - n n_i \text{Rad}(T), \quad (8)$$

where $C_i = -\frac{f a K I(T_i)}{(a-\lambda) T_i}$ represents the plasma-wall interaction, K is a uniform diffusion coefficient, $C_T = \frac{E_0^2}{\eta(T) T^{3/2}} \simeq 6.510^2 \frac{E_0^2}{Z}$, with E_0 the electric field corresponding to the loop voltage, $\eta(T)$ is the transverse Spitzer resistivity, and P_{add} is the additional power density. The above parameters of J-TEXT are used to obtain the following results and the resistivity η is considered to be a constant. Applying the following initial and boundary conditions

$$\begin{aligned} n_i(x=a) &= 0; & \left. \frac{\partial n_i}{\partial x} \right|_{x=0} &= 0 \\ T(x=a) &= T_0; & \left. \frac{\partial T}{\partial x} \right|_{x=0} &= 0 \\ n_i(t=0) &= 0; & T(t=0) &= T_0 \end{aligned} \quad (9)$$

a relation between the density limit and the target region temperature has been obtained and compared with the experimental data as shown in Fig. 7.

The PWSO 1D model also predicts the existence of a density-limit basin and a density-free basin. The J-TEXT experimental data are located in the density limit basin, as in the case of the 0D model. Within the density-limit basin, altering the start-up condition, such as increasing the pre-filled gas pressure and ECRH power at the start-up phase, should result in lower C_{III} radiation power, indicating a cleaner plasma, which leads to a higher density limit. The higher target region plasma temperature is likely a consequence of the higher power flux in the SOL, due to lower radiation inside the plasma. Additionally, the target region plasma temperature for the transition between the two basins is predicted to be higher in the 1D model ($T_t \sim 6\text{eV}$), thus allowing a more accessible density-free basin, which may be achieved in future experiments.

The lower C_{III} radiation power when using ECRH at start-up confirms the improvement of purity expected in [7] due to a central breakdown of the discharge.

5. Summary

In this work, the density limits predicted from the 0D and 1D PWSO models are compared and validated with the J-TEXT experimental data, which are located in the density-limit basin and demonstrate quantitative agreement with the PWSO model predictions under some parameter assumptions. Both theory and experiment suggest that a higher density limit corresponds to a lower impurity radiation state, which could be reached through increasing either the ECRH power or the pre-filled gas pressure at the start-up phase. In fact, due to the easy absorption of gases by carbon targets and other experimental conditions, it is difficult to start a discharge out of J-TEXT's usual start-up conditions. So, experimentally, increasing either the ECRH power or the pre-filled gas pressure at the start-up phase was not always efficient in changing

the start-up conditions. The fact that the experimental points are at the edge of the density-free regime of the 1D model indicates the possibility of reaching it by further experimental improvements in J-TEXT, despite of its graphite targets. In contrast, experiments in a tokamak with tungsten targets might enter deeply the density-free regime. Furthermore, metallic walls should enable scans of initial neutral gas density and of ECRH power with less failures and disruptions at start-up than with carbon ones.

In future, we plan to carry out more experiments to explore whether or how the J-TEXT tokamak can operate in the density-free basin predicted by the PWSO model. In the meantime, this model is being implemented in a more complete transport simulation code to predict and interpret the experimental process in a more realistic way.

6. Acknowledgment

This work is supported by the National MCF Energy R&D Program of China under Grant Nos. 2019YFE03050004 and 2018YFE0310300, the National Natural Science Foundation of China Grant No. 51821005, and the U.S. Department of Energy Grant Nos. DE-FG02-86ER53218 and DE-SC0018001. The computing work in this paper is supported by the Public Service Platform of High Performance Computing by Network and Computing Center of HUST.

Appendix A. The fitted chemical sputtering yield function

The data used to fit Eq. 6 are from Fig. 3.8a of [12] and Fig. 6 of [18]. The values of fitting coefficients are as follows: $a_1 = -0.21716823$, $b_1 = 1.49621640$, $c_1 = -3.10869745$, $a_2 = -0.55766667$, $b_2 = -0.88506667$, and $E_{1,inter} = 1.24709069$. And Fig. 8 shows the plot of original data used and the fitting function.

References

- [1] M. Greenwald, J.L. Terry, S.M. Wolfe, S. Ejima, M.G. Bell, S.M. Kaye, and G.H. Neilson. A new look at density limits in tokamaks. *Nuclear Fusion*, 28(12):2199–2207, 1988.
- [2] M. Greenwald. Density limits in toroidal plasmas. *Plasma Physics and Controlled Fusion*, 44(8):R27–R53, 2002.
- [3] P. Zanca, F. Sattin, D.F. Escande, G. Pucella, and O. Tudisco. A unified model of density limit in fusion plasmas. *Nuclear Fusion*, 57(5):056010, 2017.
- [4] P. Zanca, F. Sattin, D.F. Escande, and JET Contributors. A power-balance model of the density limit in fusion plasmas: application to the l-mode tokamak. *Nuclear Fusion*, 59(12):126011, 2019.
- [5] P. Zanca, F. Sattin, D.F. Escande, F. Auriemma, and JET Contributors. A power-balance model for the l-mode radiative density limit in fusion plasmas. *Plasma Physics and Controlled Fusion*, 64(5):054006, 2022.
- [6] G. Fuchert, S.A. Bozhenkov, N. Pablant, K. Rahbarnia, Y. Turkin, A. Alonso, T. Andreeva, C.D. Beidler, M. Beurskens, A. Dinklage, J. Geiger, M. Hirsch, U. Höfel, J. Knauer, A. Langenberg, H.P. Laqua, H. Niemann, E. Pasch, T. Sunn Pedersen, T. Stange, J. Svensson, H. Trimino Mora, G.A. Wurden, D. Zhang, R.C. Wolf, and W7-X Team. Global energy confinement in the initial limiter configuration of wendelstein 7-x. *Nuclear Fusion*, 58(10):106029, 2018.

- [7] D.F. Escande, F. Sattin, and P. Zanca. Plasma-wall self-organization in magnetic fusion. Nuclear Fusion, 62(2):026001, 2022.
- [8] T. Klinger, T. Andreeva, S. Bozhenkov, C. Brandt, R. Burhenn, and B. Buttenschon et al. Overview of first wendelstein 7-x high-performance operation. Nuclear Fusion, 59(11):112004, 2019.
- [9] R.C. Wolf, A. Alonso, S. Akaslopolo, J. Baldzuhn, M. Beurskens, C.D. Beidler, and C. Biedermann et al. Performance of wendelstein 7-x stellarator plasmas during the first divertor operation phase. Physics of Plasmas, 26(8):082504, 2019.
- [10] A. Pavone, U. Hergenbahn, M. Krychowiak, U. Hoefel, S. Kwak, J. Svensson, P. Kornejew, V. Winters, R. Koenig, M. Hirsch, K.-J. Brunner, E. Pasch, J. Knauer, G. Fuchert, E.R. Scott, M. Beurskens, F. Effenberg, D. Zhang, O. Ford, L. Vanó, and R.C. Wolf. Measurements of visible bremsstrahlung and automatic bayesian inference of the effective plasma charge Z_{eff} at W7-X. Journal of Instrumentation, 14(10):C10003, 2019.
- [11] Y. Liang, N. Wang, Y. Ding, Z. Chen, Z. Chen, Z. Yang, Q. Hu, Z. Cheng, L. Wang, Z. Jiang, B. Rao, Z. Huang, Y. Li, W. Yan, D. Li, H. Liu, L. Zeng, Y. Huang, D. Huang, Z. Lin, W. Zheng, F. Hu, K. Zhao, M. Jiang, Y. Shi, H. Zhou, S. Peng, W. Guo, L. Gao, Z. Wang, M. Zhang, K. Yu, X. Hu, Q. Yu, G. Zhuang, K. Gentle, Y. Pan, and the J-TEXT Team. Overview of the recent experimental research on the J-TEXT tokamak. Nuclear Fusion, 59(11):112016, 2019.
- [12] P. C. Stangeby. The Plasma Boundary of Magnetic Fusion Devices. CRC Press, 2000.
- [13] D. Xia, F. Cui, C. Liu, Z. Wang, Z. Yu, Y. Jin, and the J-TEXT team. The anode power supply for the ECRH system on the J-TEXT tokamak. Plasma Science and Technology, 20(1):014018, 2018.
- [14] J. Zhang, P. D. Vries, K. Nagasaki, D. Xia, W. Jiang, and Z. Wang. Electron cyclotron heating assisted start-up experiments in J-TEXT. IEEE Transactions on Plasma Science, 48(12):4397–4501, 2020.
- [15] J. Zhang, P. D. Vries, K. Nagasaki, D. Xia, W. Jiang, Z. Yang, Z. Cheng, L. Gao, X. Xu, Z. Wang, N. Wang, Y.H. Ding, Z. Chen, Z. Chen, P. Yuan, and J-TEXT Team. Experimental study of the electron cyclotron assisted start-up on J-TEXT. Submitted to Nuclear Fusion, 2023.
- [16] Y. Wang, L. Gao, P. Shi, X. Xu, Y. Zhou, Q. Yang, C. Yang, Q. Tao, C. Shen, Y. Wang, L. Wang, Z. Chen, D. Xia, Z. Chen, N. Wang, Z. Yang, Y. Ding, Y. Pan, and J-TEXT Team. Recent progress on the J-TEXT three-wave polarimeter-interferometer. Plasma Science and Technology, 24(6):064001, 2022.
- [17] Y. Yamamura and H. Tawara. Energy dependence of ion-induced sputtering yields from monatomic solids at normal incidence. Atomic Data and Nuclear Data Tables, 62(2):149–253, 1996.
- [18] J. Roth, E. Tsitrone, and A. Loarte. Plasma-wall interaction: Important ion induced surface processes and strategy of the eu task force. Nuclear Instruments and Methods in Physics Research Section B: Beam Interactions with Materials and Atoms, 258(1):253–263, 2007.

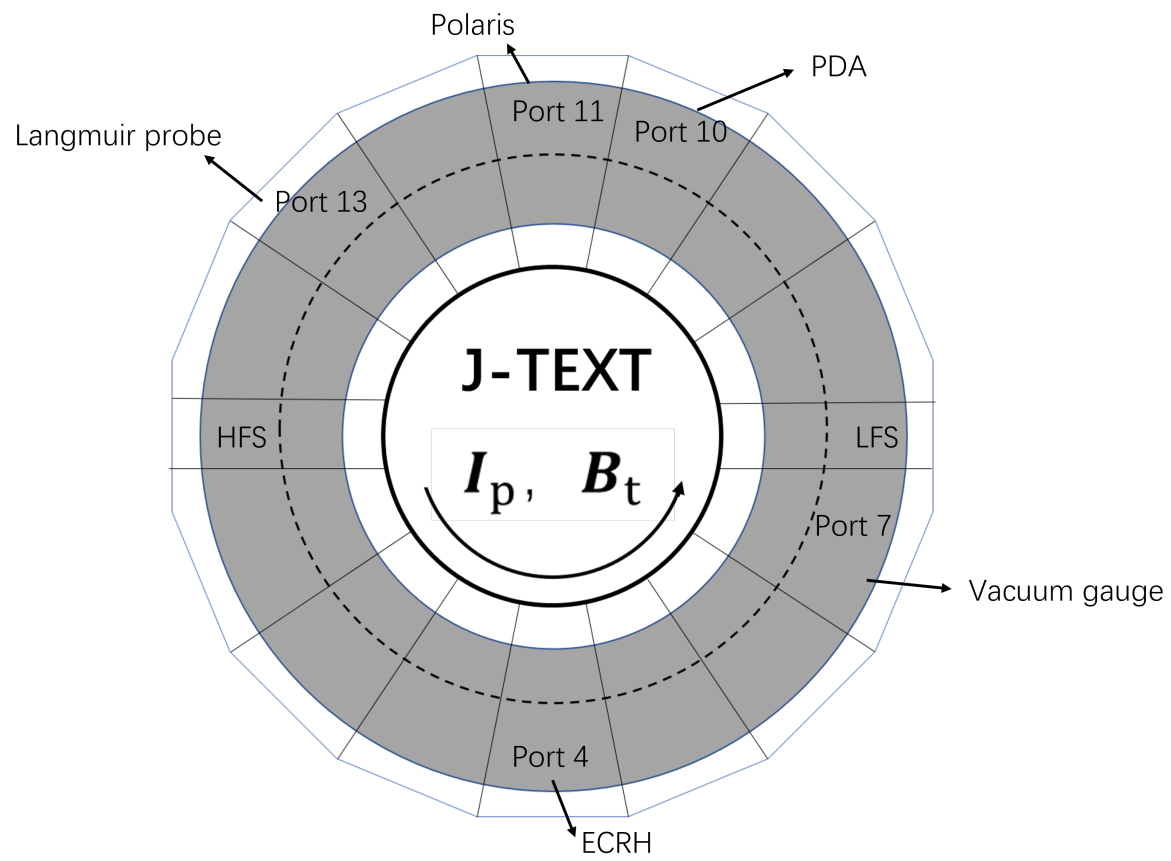


Figure 1. Top view of the relevant diagnostics on J-TEXT utilized in this study.

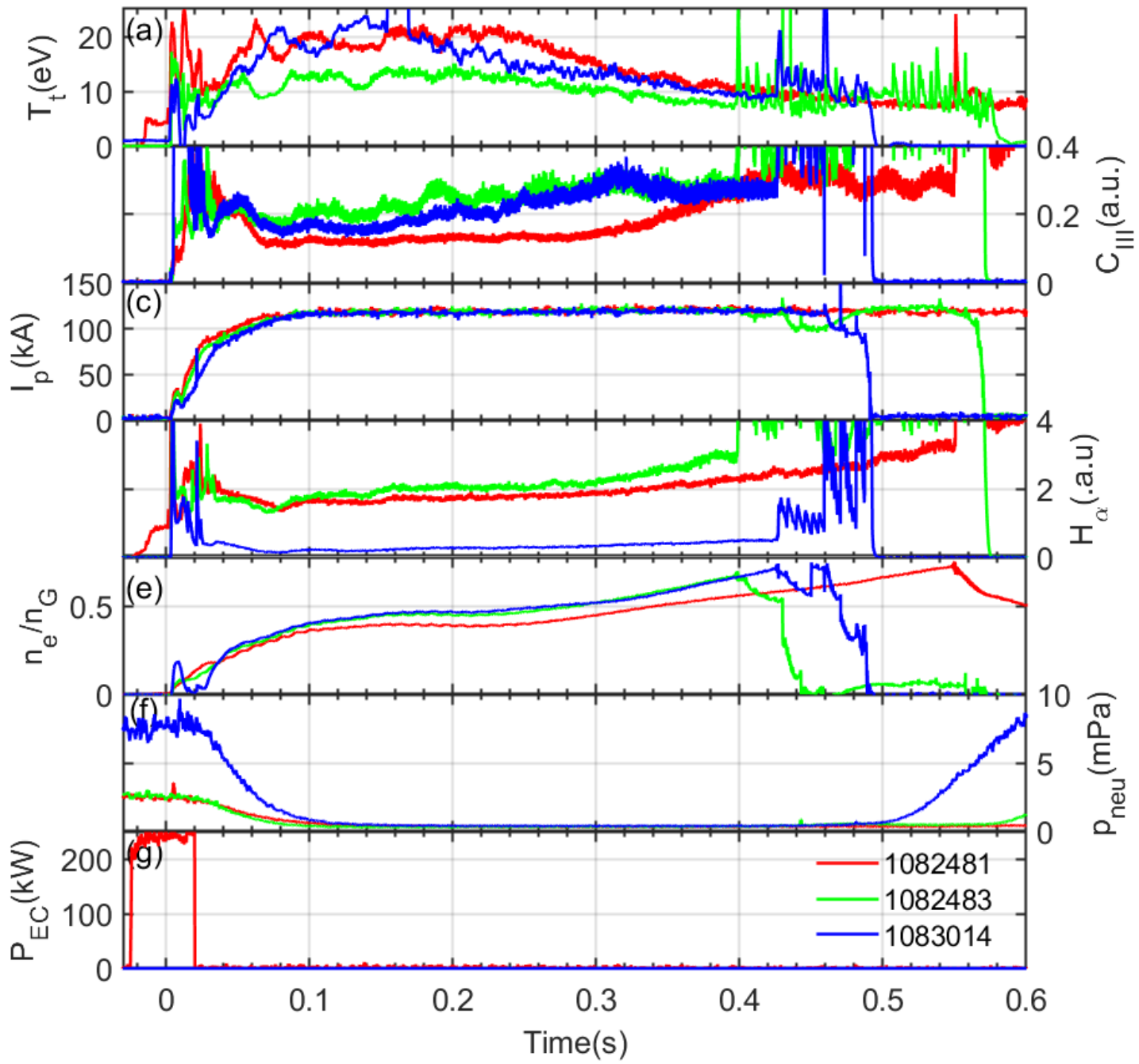


Figure 2. Time histories of key parameters in density limit experiments with various ECRH power and pre-filled gas pressure in the start-up phase.

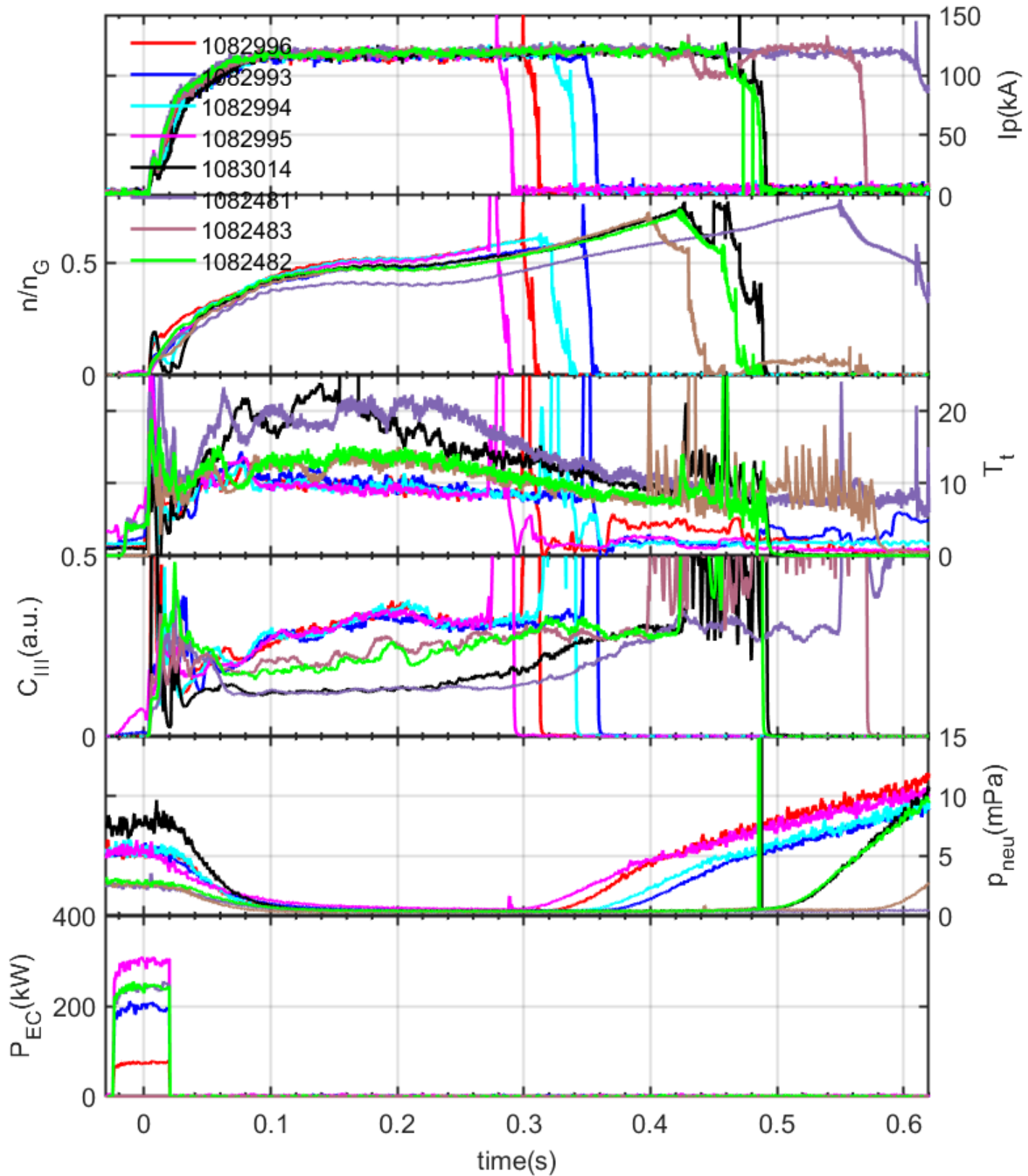


Figure 3. Time histories of key parameters in density limit experiments with various ECRH power and pre-filled gas pressure in the start-up phase and the same plasma current.

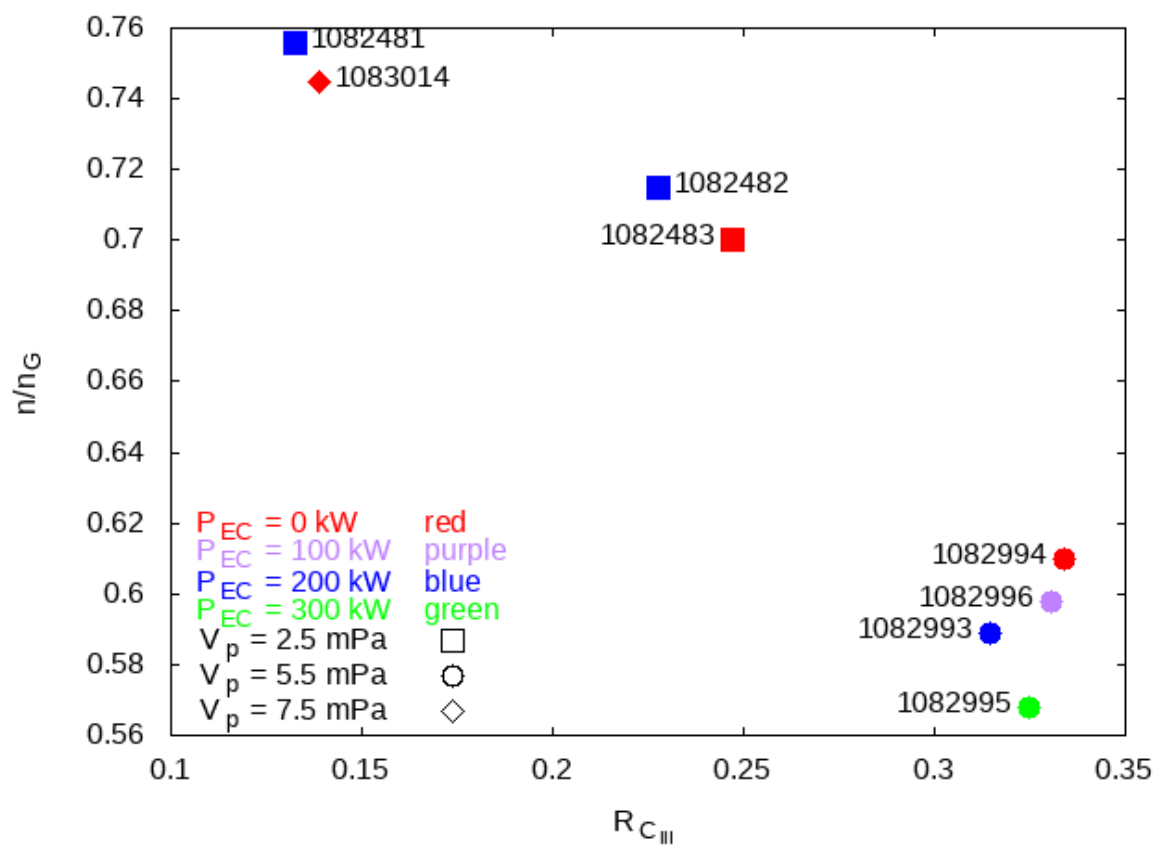


Figure 4. The density limit and the corresponding radiation power $R_{C_{III}}$ measured from experiments for varying ECRH power and pre-filled gas pressure in the start-up phase.

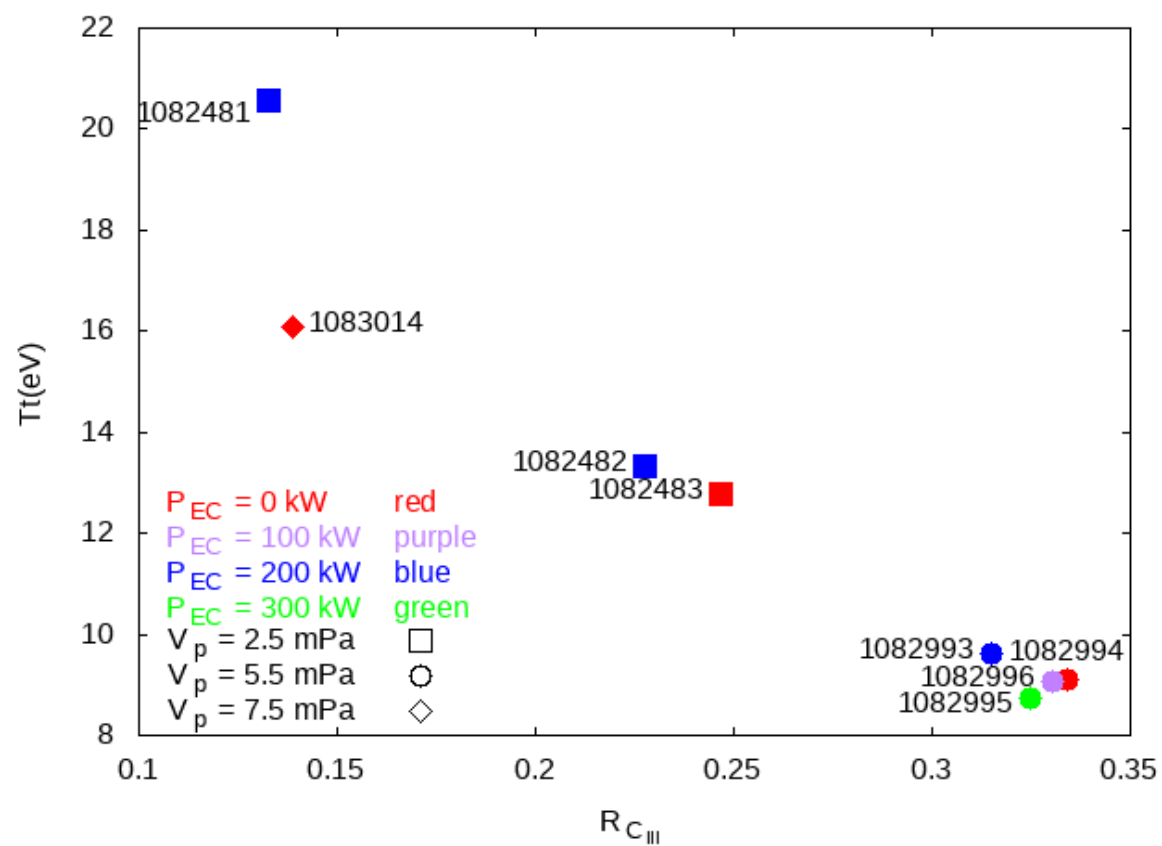


Figure 5. The plasma target region temperature T_t and the corresponding impurity radiation power R_{CIII} measured from experiments for varying ECRH power and pre-filled gas pressure in the start-up phase.

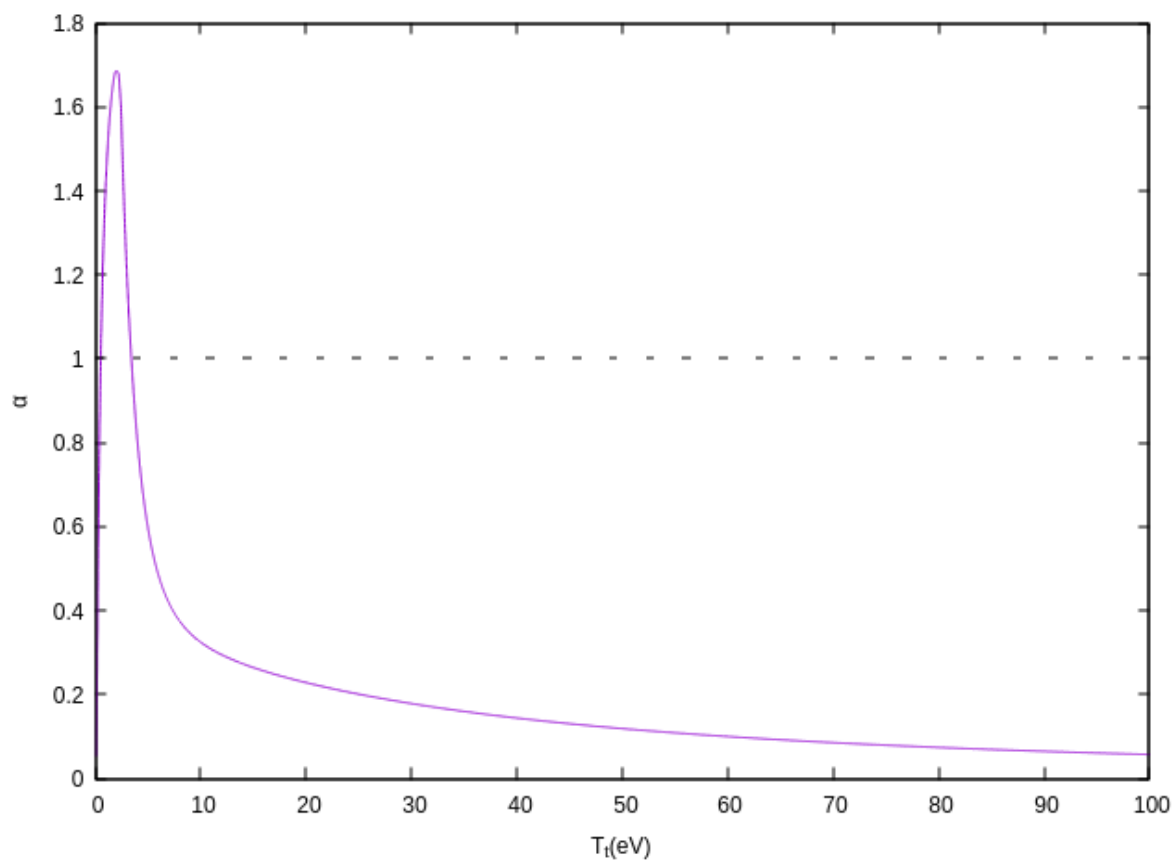


Figure 6. The coefficient α in Eq. (2) of the PWSO 0D model as a function of the target region plasma temperature for a fixed plasma density.

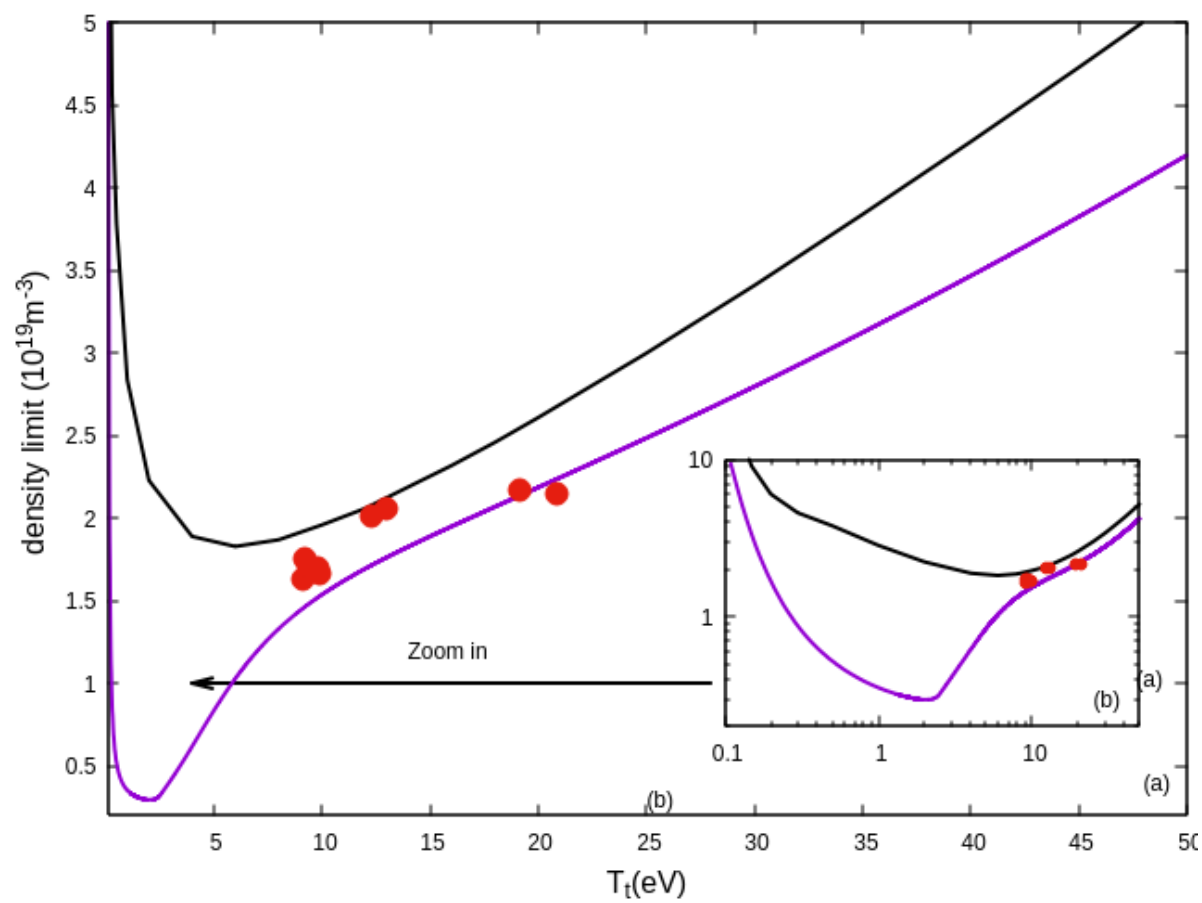


Figure 7. The density limits as functions of the target region plasma temperature T_t using (a): linear and (b): logarithmic coordinates as predicted from the PWSO 0D (purple solid line) and 1D (black line) models in comparison with the experimental data (red circular symbol).

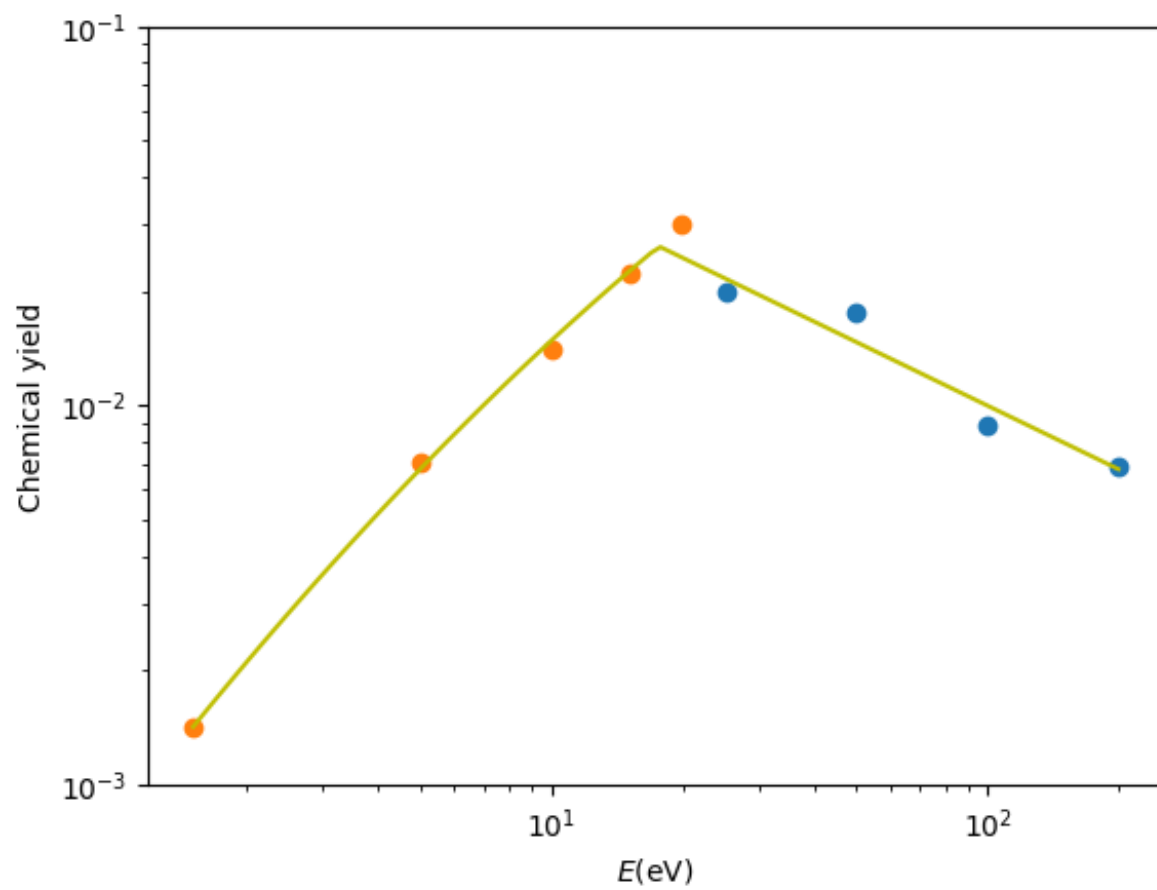


Figure 8. The fitted chemical sputtering yield function (solid line) and the original data from [12] (blue points) and [18] (orange points).